Multimode Multidrop Serial Coalescence Effects during Condensation on Hierarchical Superhydrophobic Surfaces

ARTICLE *in* LANGMUIR · DECEMBER 2012

Impact Factor: 4.46 · DOI: 10.1021/la304264g · Source: PubMed

6 AUTHORS, INCLUDING:

Konrad Rykaczewski
Massachusetts Institute of Technology
48 PUBLICATIONS **711** CITATIONS
SEE PROFILE

Sushant Anand
Massachusetts Institute of Technology
16 PUBLICATIONS **305** CITATIONS
SEE PROFILE

Xuemei Chen
Purdue University
24 PUBLICATIONS **340** CITATIONS
SEE PROFILE

Zuankai Wang
City University of Hong Kong
50 PUBLICATIONS **1,030** CITATIONS
SEE PROFILE

Langmuir

Article

pubs.acs.org/Langmuir

Multimode Multidrop Serial Coalescence Effects during Condensation on Hierarchical Superhydrophobic Surfaces

Konrad Rykaczewski,*[,†] Adam T. Paxson,[†] Sushant Anand,[†] Xuemei Chen,[‡] Zuankai Wang,[‡] and Kripa K. Varanasi*[,†]

[†]Department of Mechanical Engineering, Massachusetts Institute of Technology, Cambridge, Massachusetts 02139, United States

[‡]Department of Mechanical and Biomedical Engineering, City University of Hong Kong, Hong Kong, China

Supporting Information

ABSTRACT: The prospect of enhancing the condensation rate by decreasing the maximum drop departure diameter significantly below the capillary length through spontaneous drop motion has generated significant interest in condensation on superhydrophobic surfaces (SHS). The mobile coalescence leading to spontaneous drop motion was initially reported to occur only on hierarchical SHS, consisting of both nanoscale and microscale topological features. However, subsequent studies have shown that mobile coalescence also occurs on solely nanostructured SHS. Thus, recent focus has been on understanding the condensation process on nanostructured surfaces rather than on hierarchical SHS. In this work, we investigate the impact of microscale topography of hierarchical SHS on the droplet coalescence dynamics and wetting states during the condensation process. We show that isolated mobile and immobile coalescence between two drops, almost exclusively focused on in previous studies, are rare. We identify several new droplet shedding modes, which are aided by tangential propulsion of mobile drops. These droplet shedding modes comprise of multiple droplets merging during serial coalescence events, which culminate in formation of a drop that either departs or remains anchored to the surface. We directly relate postmerging drop adhesion to formation of drops in nanoscale as well as microscale Wenzel and Cassie–Baxter wetting states. We identify the optimal microscale feature spacing of the hierarchical SHS, which promotes departure of the highest number of microdroplets. This optimal surface architecture consists of microscale features spaced close enough to enable transition of larger droplets into micro-Cassie state yet, at the same time, provides sufficient spacing in-between the features for occurrence of mobile coalescence.

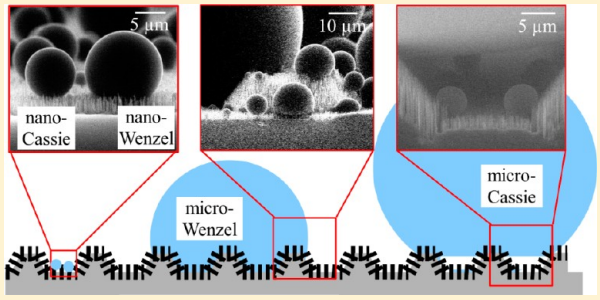

INTRODUCTION

Development of passive methods to enhance water condensation rate could dramatically improve the energy efficiency of power generation,[1−3] air conditioning systems,[4] water desalination,[5,6] and water harvesting.[7−12] The rate of this phase change process is largely limited by how quickly condensate departs the surface.[13−19] For example, the steady state condensation rate on hydrophobic surfaces, which promote formation of easily shedding droplets, is significantly higher than that on hydrophilic surfaces, which favor water film formation (i.e., dropwise vs filmwise condensation mode). On vertically inclined flat hydrophobic surfaces, hemispherical drops grow via coalescence until reaching a diameter equal to the water capillary length of about 2.7 mm.[13,16] Subsequently, the drops slide off the surface due to gravity. Recently, Chen et al.[20] and Dorrer and Ruhe[21] observed that during condensation on properly designed superhydrophobic surfaces (SHS)[22] drops with sizes significantly below the capillary length can depart the surface via spontaneous droplet motion.[2,20−30] The prospect of enhancing the condensation rate by decreasing the maximum departure diameter, which could double the heat transfer rate,[2,13,16,31,32] has generated much interest and research effort in condensation on SHS.

Boreyko and Chen[23] initially reported that hierarchical SHS, which consist of both nanoscale and microscale topological features, are necessary to promote spontaneous drop motion.[23] More recently this mode of condensation has also been observed on solely nanostructured surfaces.[2,21,22,25,28,29,33,34] Rykaczewski et al.[22,35] found that the primary role of the nanostructure is confinement of the base area of nucleating droplets, which leads to formation of nearly spherical microdroplets through contact angle increase. In a subsequent work, Enright et al.[34] reached a similar conclusion by studying the effect of the nanoscale SHS architecture on later stages of microdroplet growth. Similarly, Liu et al.[36] found in their theoretical study that the nanostructure is crucial for formation of high contact angle microdroplets. Rykaczewski[35] demonstrated that the forming droplets grow in purely constant base area mode until reaching a contact angle of 130° to 150°. The

Received: October 27, 2012
Revised: December 13, 2012
Published: December 21, 2012

author found that subsequently the drops grow through cyclic stick-and-slip triple line contact motion until coalescing with neighboring drops. Miljkovic et al.[33] found that the growth rate of droplets in the wetting Wenzel[37] state is much higher than of those in the nonwetting Cassie−Baxter[38] state. This behavior is primarily due to a significant increase in the base area of droplets, and with that number of silicon pillars in contact with the liquid, when the drops transition from the Wenzel to the Cassie−Baxter state.

Other studies of condensation on nanostructured SHS have focused on the physical mechanism and factors enabling the spontaneous drop motion. Boreyko and Chen[23] reported that this motion is normal to the substrate surface and is triggered by coalescence of two developed high contact angle microdroplets. Specifically, the authors found that two such microdroplets with diameters above 10 μm can become mobile after coalescence due to release of excess surface energy during the event. Subsequently, Wang et al.[24] found that the 10 μm droplet diameter threshold is necessary for the surface energy released during coalescence to dominate over viscous dissipation and the gravitational-potential energy. A more in-depth theoretical model of this process involving two to three drops has been recently published by Liu et al.[39] From an experimental perspective, He et al.[28] and Feng et al.[29] found that surface morphology and chemistry significantly impact the ability of two droplets with diameters below 100 μm to induce postcoalescence motion on nanostructured aluminum and copper SHS, respectively. Both of the groups attributed higher frequency of mobile coalescence events to the nanostructured SHS which promote transition of droplets into nonwetting Cassie−Baxter state.[38] However, the authors did not provide any direct evidence of droplet transition into this wetting state.

The influence of microscale topography on wetting states of sessile and impinging drops on SHS has been studied extensively.[40−59] Similarly, numerous studies explored condensation dynamics on solely microstructured SHS.[10,42,60−68] However, the impact of microscale topography on coalescence dynamics during condensation on hierarchal SHS has only been explored theoretically by Liu et al.[36,39] and experimentally by Chen et al.[27] Using thermodynamic analysis, Liu et al.[36,39] predicted that the microscale topography should influence the final wetting state, apparent contact angle, rolling angle, and departure diameter of a condensed drop. Chen et al.[27] focused on how the microscale topography affects cumulative departure volume and drop number density. In this work, we investigate the impact of microscale topography on the droplet coalescence dynamics and wetting states during the condensation process. We image condensation occurring on hierarchical SHS consisting of microscale truncated cones with varied dimensions and pitch covered by dense array of nanotrees (NTs)[22,27,69] across multiple length and time scales using environmental scanning electron microscopy[70−72] (ESEM) and high speed light microscopy. We show that isolated mobile and immobile coalescence between two drops, almost exclusively focused on in previous studies, are rare. The majority of coalescence events on hierarchical SHS occurs in series and leads to merging of multiple droplets. These drops can merge locally or be sequentially swept up in domino-like process. Such multidrop serial coalescence events are triggered by mobile coalescence events resulting in formation of a tangentially flying droplet that subsequently collides with another neighboring or distant drop. Regardless of the number of merging drops, the serial coalescence events culminate in formation of a drop that either departs or remains anchored to the surface. We quantify the frequency of formation of the departed and anchored drops in different size regimes as a function of the microscale topography. We explain the observed postmerging drop adhesion trends through direct correlation to formation of drops in nanoscale as well as microscale Wenzel and Cassie−Baxter wetting states. We find that optimally designed hierarchical SHS, which promote the highest number of departing microdrops, consists of microscale features spaced close enough to enable transition of larger droplets into micro-Cassie state, yet at the same time provide sufficient spacing in-between the features for occurrence of mobile coalescence.

EXPERIMENTAL METHODS

Superhydrophobic Surface Fabrication Procedure. The microscale features were patterned using standard photolithography.[27] Tetramethylammonium hydroxide (TMAH) was used for anisotropic etching of silicon. Because the etching rate of the ⟨100⟩ plane was significantly faster than of the ⟨111⟩ plane, the ⟨111⟩ plane defined the microscale features, resulting in a 54.7° angle between the etched wall and the flat surface. The etching rate of the ⟨100⟩ plane using 25% TMAH solution at 80 °C was about 0.33 μm/min. The truncated cone-like silicon pillars were fabricated by carefully adjusting the etching time. Afterward, the silicon nanotrees (NTs) were fabricated using a modified Bosch deep reactive ion etching (DRIE) process. First, a thin film of fluoride polymer was deposited on the solid surface in the passivation cycle, followed by etching cycle. We carefully tuned the ratio of the etching and passivation times to leave behind residual polymer particles which served as a random nanomask for the subsequent etching. The NTs were formed by alternating etching and passivation steps. The coil power was set to ∼550 W. The chamber pressure and temperature was kept at ∼4 Pa and ∼20 °C. In the passivation cycle, the C_4H_8 flow rate was ∼85 cm^3/min. In the etching cycle, the SF_6 flow rate was ∼70 cm^3/min and platen power was set to ∼15 W. The NTs with diameter of about 400 nm, pitch of about 700 nm, and height of about 2600 nm were produced after 20 processing cycles. All the surfaces were modified by immersing in 1 mM hexane solution of perfluorooctyl trichlorosilane for about 30 min, followed by heat treatment at about 150 °C in air for 1 h.[69] This procedure resulted in a uniform coating of the nanostructures with the hydrophobic layer. Flat silicon wafers modified using this procedure had a static water contact angle of about 110°.[69] SEM images of typical NTs and the hierarchical SHS are shown in Figure 1, panels a and b−e, respectively. The dimensions and wetting parameters for these hierarchal SHS are specified in Table 1 (for details of wetting parameter calculations see the Support Information). Henceforth, we identify each of the surfaces by the center-to-center distance between the microscale features (i.e., P-120 stands for the SHS with 120 μm center-to-center distance; P-0 refers to the surface consisting only of NTs). The macroscopic contact angles were measured with a goniometer (Rame-hart model 590) using volume addition and subtraction method. First, a 1 μL sessile drop of deionized water with resistivity of 18 MΩ was deposited on the surface. To measure the advancing contact angle, measurements were taken while water was added to the drop at a rate of 0.2 μL per second. The receding contact angles were measured while volume was withdrawn from the drop at the same rate. All reported values were averages of measurements taken in four different locations on the samples. The uncertainties, which were calculated with a coverage factor of 1, were 4° for the P-0 surface and 1° for all other surfaces.

ESEM Imaging Procedure. The dynamics of water condensation were imaged using a FEI Quanta 200 FEG ESEM. The sample was mounted using vacuum compatible carbon tape on a custom-made copper sample holder at 0° or 85° to 90° corresponding to top-down and side-on imaging (see Figure 2a).[25,26,35] Sustained condensation at stable sample temperature and chamber pressure was achieved using the procedure described in detail by Rykaczewski.[35] To prevent any electron beam heating effects,[70] the drops were imaged with electron

dx.doi.org/10.1021/la304264g | Langmuir 2013, 29, 881−891

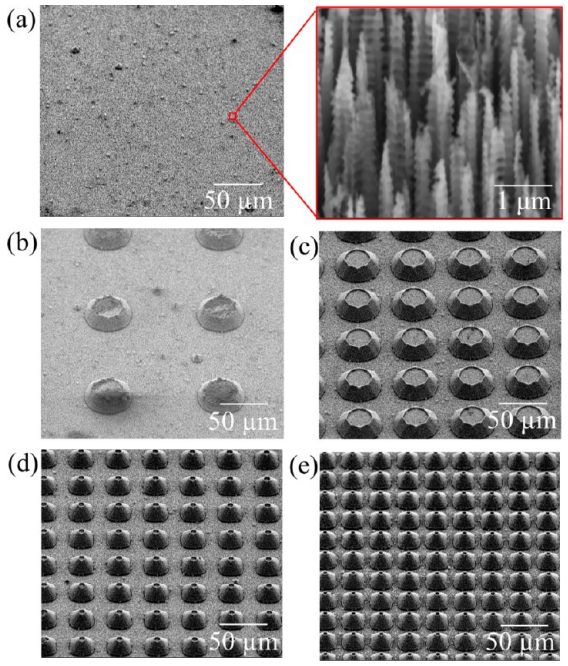

Figure 1. SEM images of (a) surface consisting only of nanotrees (P-0), and (b–e) hierarchical superhydrophobic surfaces consisting of nanotrees and truncated microcones with a center-to-center distance of (b) 120 μm (P-120), (c) 64 μm (P-64), (d) 40 μm (P-40), and (e) 30 μm (P-30). The samples were inclined at an angle of 52° from the horizontal axis.

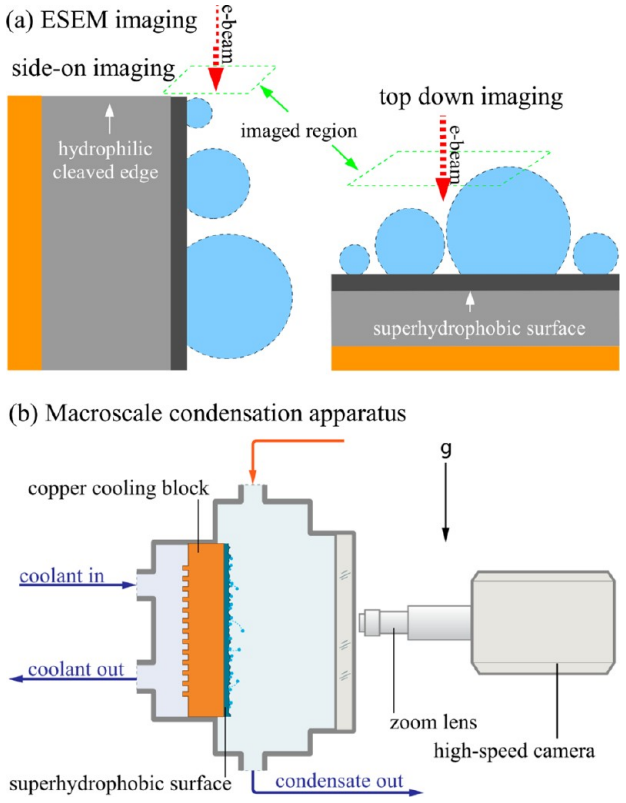

Figure 2. Schematic of (a) sample orientation during side-on and top-down ESEM imaging and (b) macroscale condensation apparatus; steam enters via port on top of chamber, condenses onto a superhydrophobic surface affixed to a copper block which is cooled by chilled water, and condensate exits through port on bottom of chamber. The condensation process is recorded by a high-speed camera.

beam energy and current of 10 keV and 0.16 nA, respectively. The dynamics of the condensation process were imaged with a dwell time of 1 μs per pixel and 512 pixel by 471 pixel frame sizes. The corresponding images were saved every 0.2 s. The captured ESEM images were analyzed using the ImageJ analysis software package.[73] The reported diameter, d, of the drops was calculated from the top-down images according to $d = 4A/p$, where A is the area and p is the perimeter of the drop. The associated standard error, σ_d, was calculated according to $\sigma_d^2 = ((4/p)\sigma_A)^2 + (-(4A)/(p^2)\sigma_p)^2$. All reported values were averages of six measurements with associated uncertainties calculated with a coverage factor of 1.

High Speed Light Microscopy. Macroscale condensation experiments were performed in a custom built condensation apparatus illustrated in Figure 2b. The superhydrophobic substrates were affixed to a copper cooling block using copper adhesive tape to ensure adequate thermal contact. The other side of the copper cooling block was cooled by a flow of chilled water supplied by a heat exchanger (Neslab II, Thermo Scientific). Before condensing, the chamber was evacuated to a pressure below 13 Pa to minimize the effect of noncondensable gases. Steam was introduced to the chamber by an electric boiler (SR-20, Reimers Boiler Co.) at a constant pressure of about 75 kPa and temperature of about 92 °C. While the subcooling of the cooling copper block was about 10 °C, it is difficult to estimate the subcooling of the superhydrophobic surface because of the unknown thermal resistance of the tape adhesive and the sample itself. Videos were recorded at 500 frames per second and 12000 frames per second by a high-speed camera (SA-1, Photron) equipped with a zoom lens (Model 6265, Navitar) and illuminated by a concentric ring light (Dolan-Jenner). For comparing condensation characteristics of the different surfaces, droplet size distribution was analyzed during later stages of condensation process dominated by coalescence regime.[74] From the videos recorded at 500 frames per second (Movies S1–S5), ~3000 frames were extracted. From these, every 100th frame was subsequently analyzed using ImageJ after performing image segmentation and thresholding.[73] To obtain droplet size distribution, droplet diameters were categorized with intervals of 30 μm. For each interval, the number of droplets in that range occurring in all the analyzed frames were counted and divided by the total number of droplets in all the analyzed frames to obtain the percentage distribution of that droplet size. Thus the droplet size distribution

Table 1. Hierarchical SHS Dimensions and Wetting Roughness Parameters[a]

sample	P	H	D_b	D_t	θ_a	θ_r	φ	$r_{micro\text{-}Wenzel}$	$r_{micro\text{-}Cassie}$	$r_{nano\text{-}Cassie}$	$r_{nanomicro\text{-}Cassie}$
P-120	120	14	51	34	165.3°	161.0°	0.13	1.07	0.06	0.26	0.016
P-64	64	12.6	49	27	164.8°	162.8°	0.32	1.17	0.14	0.26	0.036
P-40	40	14	27	7.3	163.8°	159.3°	0.20	1.25	0.026	0.26	0.007
P-30	30.2	13.4	23.8	5.4	165.5°	162.3°	0.25	1.35	0.025	0.26	0.007
P-0					164.3°	144.8°				0.26	

[a]Unless otherwise specified, the units are in micrometers. P, H, D_b, and D_t stand for center-to-center distance, height, and bottom and top diameters of the microscale features, whereas θ_a, θ_r, φ, and r refer to the macroscopic advancing contact angle, receding contact angle, volumetric solid fraction, and the Cassie or Wenzel wetting parameters on the specified length scale.

dx.doi.org/10.1021/la304264g | Langmuir 2013, 29, 881–891

averaged over a period of time could be obtained for each surface for comparison purpose. The diameters of droplets involved in isolated and serial coalescence events in 500 frames (two sets of 250 frames selected from the ~3000 frames for each surface) were measured manually. For the drops which remained anchored to the surface, the final drop diameter and number of merging drops was recorded. For the merging events which culminated in drop departure, the final drop diameter was estimated from the measured diameters of the merging drops.

RESULTS AND DISCUSSION

To confirm the occurrence of mobile coalescence events, we imaged the condensation process at 12000 frames per second using a high speed camera placed on the side of the SHS. The images in Figure 3a show postcoalescence out-of-plane droplet

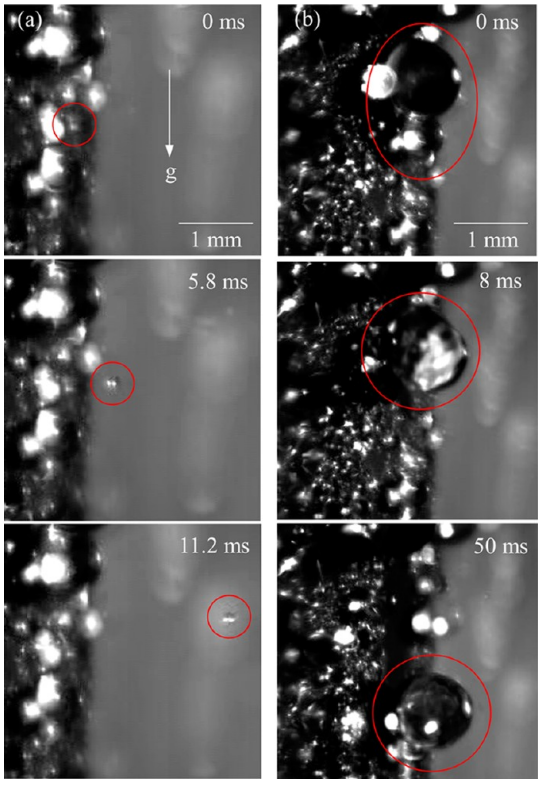

Figure 3. High speed light microscopy showing examples of mobile coalescence water droplets on P-40 superhydrophobic surface resulting in (a) out-of-plane droplet ejection and (b) rolling or shedding with gravity.

motion,[23] but the images in Figure 3b show that after coalescence larger droplets can also roll or shed with gravity in the vicinity of the surface. In the following sections we describe in depth our investigation of the impact of microscale topography on the droplet coalescence dynamics and wetting states during the condensation process.

Coalescence Dynamics on Hierarchical Superhydrophobic Surfaces. We first studied coalescence of droplets with diameters below ~45 μm using top down ESEM. We observed that coalescence of two droplets in this size regime can, but does not necessarily, lead to mobility of the newly formed drop (see Figure 4. panels a and b). To determine the threshold droplet size for mobile coalescence, we measured the diameters of closely sized coalescing droplets on all the studied surfaces. The small vs large diameter of coalescing droplets on the P-40 surface are plotted in Figure 4c (see Figure 1 in the

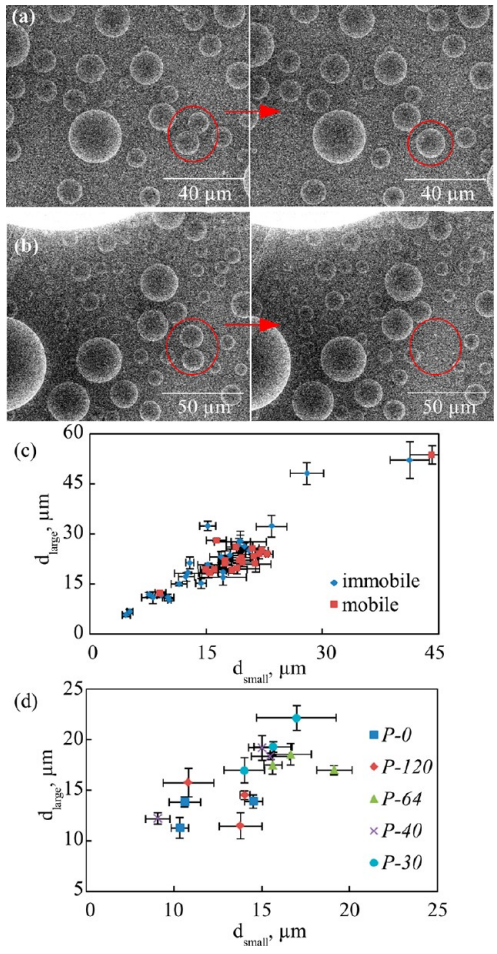

Figure 4. Top-down ESEM images of (a) immobile and (b) mobile coalescence. (c) Example plot of smaller vs larger diameter (d_{small} vs d_{large}) of two droplets involved in mobile and immobile coalescence events occurring on the P-40 surface, and (d) mobile coalescence threshold: plot of d_{small} vs d_{large} of three mobile coalescence events involving the smallest observed droplets for each surface.

Support Information for data for all SHS). A mobile coalescence threshold of about 10 to 15 μm is evident. Similarly, the plot in Figure 4d demonstrates a 10–20 μm mobile coalescence threshold for all the studied hierarchical SHS. This value is in close agreement with previous experimental[22,23,27–29,33,34] and theoretical[24,39] results.

Top-down imaging of the condensation process using high speed optics revealed several droplet shedding modes (see Figure 5 and Movies S1–S5). These events can consist of multiple neighboring drops merging locally (Figure 5a) or drops being sequentially swept up in a domino-like process across distances of even several millimeters (Figure 5, panels a–f). The multidrop merging events were likely triggered by mobile coalescence, resulting in formation of a flying droplet that subsequently collided with another neighboring or distant drop (see Figure 5, panels a, c, and g–i). The spontaneous droplet motion is typically described as being purely normal to the surface,[24,39] but to trigger the serial coalescence the droplet motion must contain a tangential component (see schematics in Figure 5, panels f and g). The tangential component of the droplet's motion could be caused by coalescence of uneven sized drops, precoalescence tangential movement of one of the drops,[23] or asymmetric adhesion of the droplets to the

dx.doi.org/10.1021/la304264g | Langmuir 2013, 29, 881–891

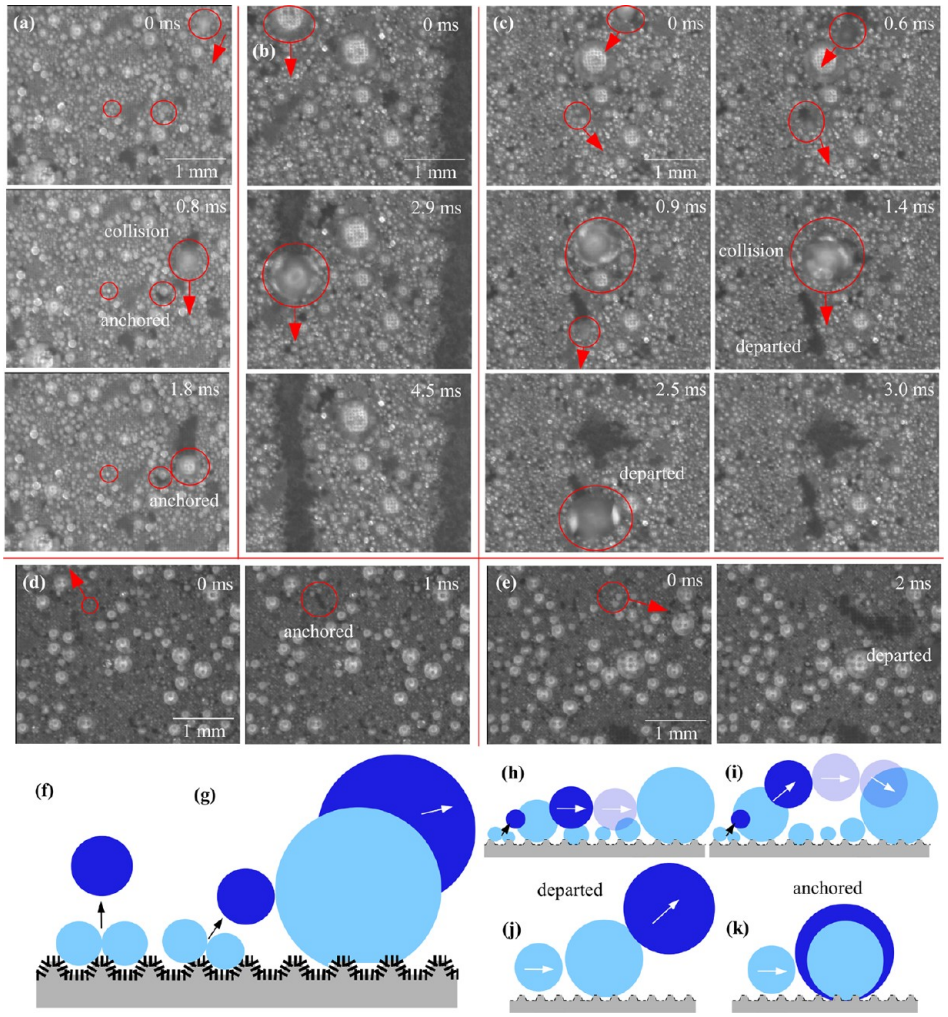

Figure 5. High speed light microscopy images showing examples of serial coalescence events resulting in merging of multiple droplets that culminate in formation of (a and d) an anchored drop and (b, c, and e) a departed drop. Note that large droplets can depart the surface in shedding mode as in (b) as well as in jumping mode in (c and e); Schematics of mobile coalescence involving two drops with (f) purely out-of-plane motion and (g) motion containing a tangential component which results in collision and dislodging of neighboring droplet, which in turn can trigger (h) domino-like sweeping coalescence or (i) nonlocalized collision coalescence, both of which can culminate in formation of a (j) departed or (k) anchored drop.

microscale topological features. Once triggered, the domino-like serial coalescence can sweep up droplets in any direction. For example droplets in Figure 5a–c and Figure 5 d were swept with and against gravity while those in Figure 5e were swept laterally. However, we observed that serial coalescence events involving drops with diameters larger than about 300 μm typically resulted in the drops shedding with gravity. Also, such drops did not necessarily sweep up all droplets in their path (Figure 5, panel b vs c), but it was difficult to determine whether in the sweeping mode the droplets remained in contact with or were slightly detached from the substrate. Irrelevant of the mode, ultimately the isolated and serial coalescence events resulted in formation of a drop that had either departed or remained anchored to the surface (Figure 5, panels h vs i).

To study postmerging drop adhesion to the hierarchical SHS, we quantified the number of serial coalescence events which culminated in formation of a drop which had departed or remained anchored to the surface from 500 high speed optical images collected during one second of operation of the condensation apparatus. The results presented in histograms in Figure 6 specify the number of drops involved in these events as well as the diameter range of the final droplet (30–100, 100–200, and above 200 μm). These results highlight the predominance of serial coalescence events over isolated coalescence events. Specifically, isolated coalescence events occurred almost solely for droplets with merged diameter in the 30–100 μm range and even in this size regime comprised of at most 15% of the total drop merging events. The majority of coalescence events in this size regime were serial and involved between three and six droplets. For the P-0, P-120, P-40, and P-30 about 30% of the drop merging events that produced drops with diameters in the range 30–100 μm ended with departure of that drop. In contrast, on the P-64 surface about 60% of drop merging events producing drops in this size regime ended with departure of the drop. The percentage of departing drops with diameters in the 100–200 μm and above 200 μm ranges varied from 0% to 45% and 0% to 63%, respectively. We did not observe any clear relation between the microscale topography and merged drop adhesion in this size regime.

Droplet Wetting States on Hierarchical Superhydrophobic Surfaces. To gain an insight into the physical mechanism of postmerging drop adhesion to the SHS, we investigated the droplets wetting states occurring on these surfaces. Following Verho et al.,[59] we distinguished droplet

dx.doi.org/10.1021/la304264g | Langmuir 2013, 29, 881–891

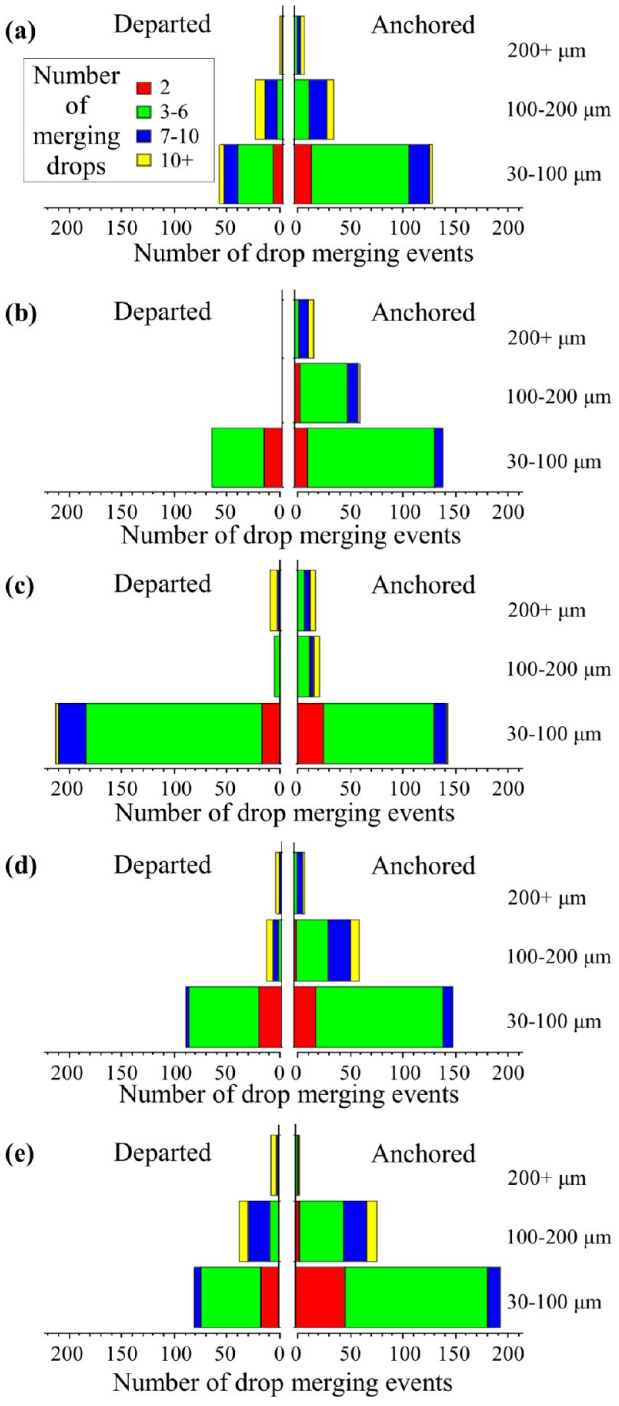

Figure 6. Analysis of isolated (2 drop) and serial (more than 2 drops) drop merging events culminating in formation of a drop in the range of 30 to 100 μm, 100 to 200 μm, and above 200 μm regime which departed or remained anchored to the (a) P-0, (b) P-120, (c) P-64, (d) P-40, and (e) P-30 surfaces during one second of condensation in the condensation apparatus. The number of droplets involved in the droplet merging events is also indicated.

wetting of the nanoscale and the microscale topological features illustrated in Figure 7a as nano-Wenzel, nano-Cassie, micro-Wenzel, and micro-Cassie states. We note that droplets in the microlevel states can also locally wet the nanostructure through formation of nanoscale capillary bridges. Miljkovic et al.[33] and Rykaczewski et al.[22,35,75] previously observed formation of microdroplets with diameters below ~20 μm in the nano-Wenzel as well as the nano-Cassie states. We confirm their results with the side-on ESEM images in Figure 7, panels c and d (also see Movies S6–S10), which clearly show droplets in both of these wetting states. The final wetting state of the microdroplets depends on the location of nucleation of nanodroplets, which combine to form the larger droplets.[22,35,70,71] The side-on ESEM image in Figure 7 b demonstrates that the nanodroplets can nucleate on bottom as well as on top of the nanotrees, yielding microdroplets in nano-Wenzel and nano-Cassie states. Irrelevant of the wetting state, microdroplets with diameters greater than 10 μm grow primarily by coalescence with neighboring droplets. Merging of two microdroplets in the nano-Cassie state is much more likely to result in the postcoalescence motion.[33,39] If a microdroplet in the nano-Wenzel state is involved in a coalescence event, it can serve as an anchor and prevent the newly formed drop from moving.

We observed that formation of droplets in the micro-Wenzel and the micro-Cassie states is intimately related to the geometry of the microscale topography. The close up ESEM images in Figure 7e clearly show that large droplets on the P-64, P-40, and P-30 surfaces can bridge tops of the microcones without penetrating the space in-between them (also see Movies S6–S10). Moreover, we were able to image formation of multiple smaller droplets within the gaps below the large droplet. In contrast, on the P-120 surface all the larger droplets filled-in the volume in-between the microscale features. To confirm the direct side-on ESEM observations with a larger number of droplets, we evaluated the brightness of the droplets observed using top-down light microscopy. Droplets in the micro-Cassie state appear brighter because they have a smooth bottom water-gas interface and reflect light in a mirror-like specular fashion (see Figure 7e).[76] In turn, droplets in the micro-Wenzel state appear darker because they have a rough bottom interface and reflect light in a diffuse fashion (see Figure 7e).[76] Using this approach, we confirmed that the micro-Cassie state occurs only on the SHS with the center-to-center distance of the microscale features equal or smaller than 64 μm. Furthermore, we observed that in order to be in the micro-Cassie state droplets had to have diameters of at least 120–160, 100–140, and 80–120 μm on the P-64, P-40, and P-30 SHS, respectively. In other terms, the droplets had to have diameters two to three times greater than the center-to-center distance between the microscale topological features. We also observed that on the micro-Cassie enabling surfaces the maximum observed drop diameter is only ~500 μm as compared to the ~1000 μm observed on the P-120 and the P-0 surfaces. However, not all larger droplets formed during sequential coalescence events on the micro-Cassie enabling surfaces departed because of the nanoscale capillary bridges forming between the drop and the tops of the microscale features (see Figure 7, panels f and g). A random number of these capillary bridges form due to coalescence with satellite microdroplets in nano-Wenzel state.[25,62,63] The capillary bridges significantly increase the local adhesion force and thus can act as anchors preventing merged droplet departure.

Relation between Postmerging Drop Adhesion and Its Wetting State. We re-evaluated the postmerging drop adhesion on the hierarchical SHS in light of the wetting states of condensed droplets. Specifically, we recasted the absolute size data in Figure 6 in scaled form of merged droplet diameter to microscale topography center-to-center distance ratio (d_{drop}/P). The cumulative number of departed and anchored drops

dx.doi.org/10.1021/la304264g | Langmuir 2013, 29, 881–891

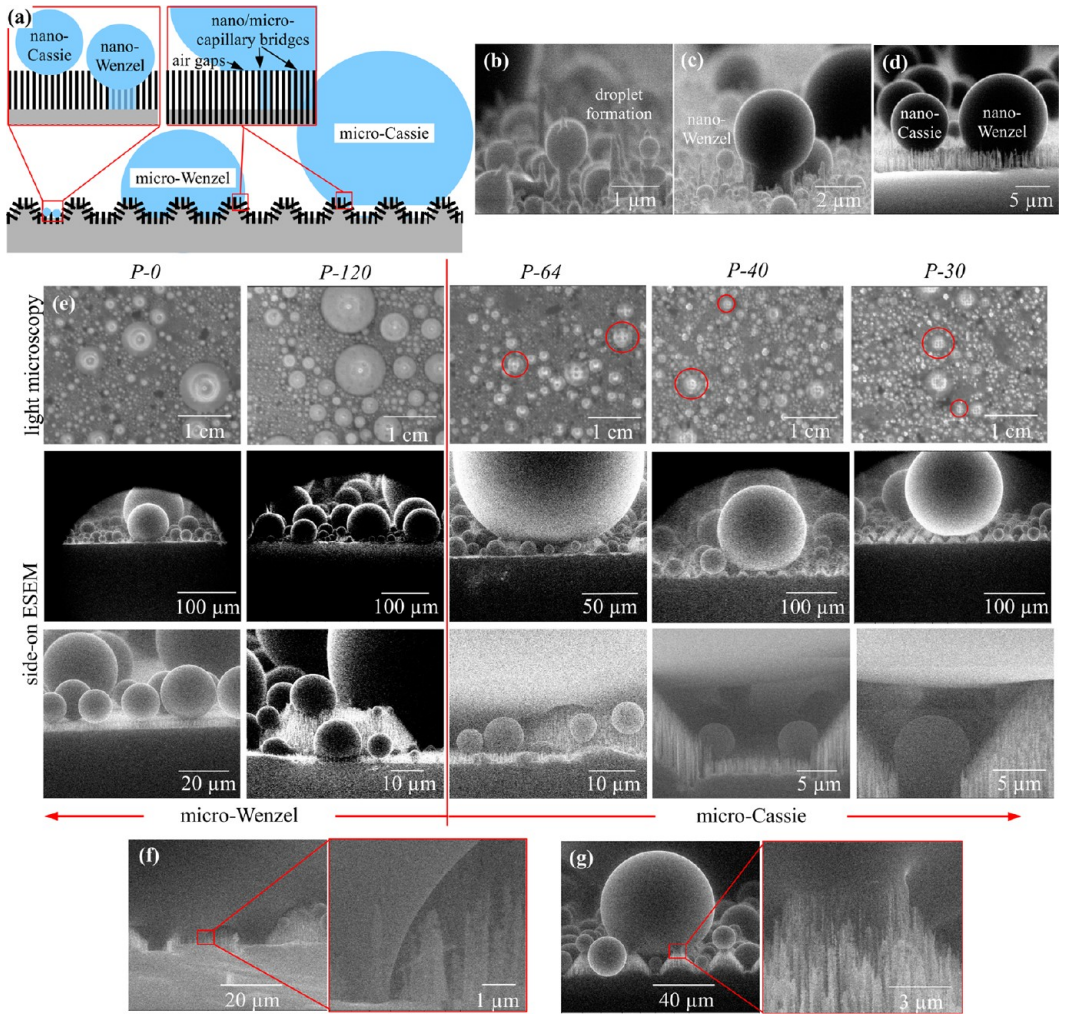

Figure 7. Possible wetting states of droplets condensed on a hierarchical superhydrophobic surface: (a) representative schematic, (b–d) side-on ESEM images of example droplets condensed on the nanotrees in nano-Wenzel and nano-Cassie states, (e) light microscopy and side-on ESEM images of water droplets in micro-Wenzel and micro-Cassie states; the red circles mark smallest observable drops in the micro-Cassie state, and (f and g) close-up examples demonstrating formation of capillary bridges between larger droplets and the nanoscale topography.

are plotted in Figure 8 a and b. We observe that irrelevant of their absolute number, the cumulative number of departing drops saturates for all samples at d_{drop}/P ratio of two to three. Since this value of d_{drop}/P is also the minimum threshold for occurrence of the micro-Cassie state, we used to define a border between "small" and "large" merged drops in the histogram in Figure 8c. No large droplets depart the P-120 surface, because they remained anchored in the "sticky" micro-Wenzel state. In contrast, on all of the micro-Cassie enabling surfaces about 20–25% of the drop merging events resulted in formation of a large drop which departed the surface (see Figure 8d). This general observation implies that adhesion of Cassie-state droplets condensed on hierarchical SHS is governed by the number of microscale features in contact with the drop. For the small droplets, the percentage of departed drops was unaffected by the microscale topological features with the exception of P-64 surface. On this hierarchical SHS the fraction (Figure 8c) and the total number of small departing drops (Figure 8a) was two to three times higher than on any of the hierarchical SHS as well as the solely nanostructured P-0 surface (25–35% of drops depart this surface after coalescence). This trend is also reflected in the rather uniform drop size distribution curve for the P-64 surface in Figure 8d. Because of their efficient shedding, the percentage of small drops on the P-64 surface is less than on the other surfaces.

The microscale topological features on the P-64 surface are spaced closely enough to enable transition of large droplets into the micro-Cassie state, while at the same time providing sufficient space in-between the features for coalescence of two small droplets with diameters above d_{th} (see Figure 9b). As a result mobile coalescence can occur between two small drops condensed in-between the features. Consequentially, the mobile droplets can trigger numerous multidrop merging events that lead to formation of easily departing drops in the micro-Cassie state. In contrast, the schematic in Figure 9a illustrates that on surfaces with $P < 2d_{th}$ (P-40 and P-30 SHS), only microdroplets with diameter below d_{th} can coalesce in-between the features, decreasing the number of mobile coalescence events between small drops. In addition the probability of mobile coalescence events decreases in this case because the edges of the microscale topological features are more prone to defects in the nanostructure. Lastly, despite large solely nanostructured area, we do not observe numerous small departing drops on the P-120 surface because large fraction of

dx.doi.org/10.1021/la304264g | Langmuir 2013, 29, 881–891

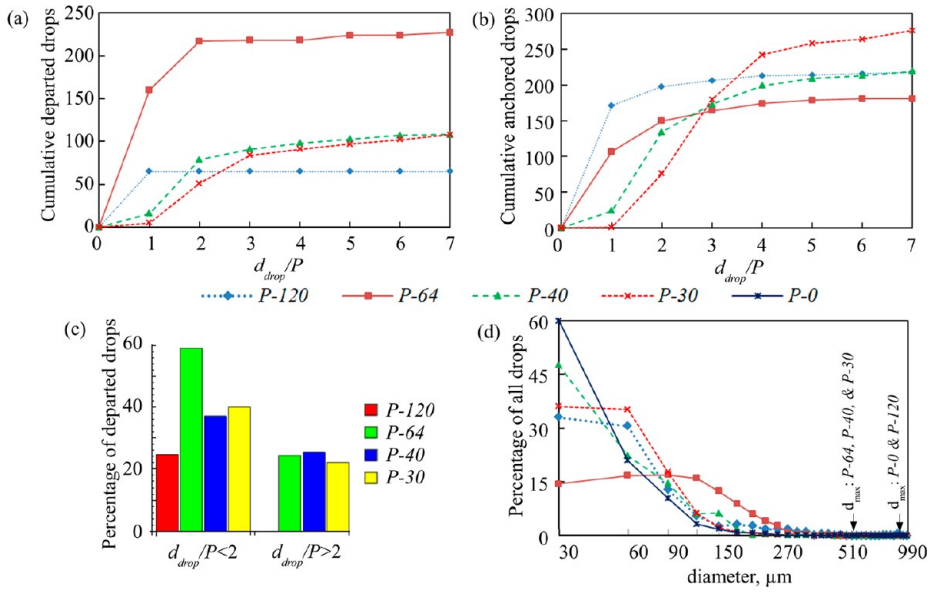

Figure 8. Cumulative number of drops which have (a) departed or (b) remained anchored to the surface in terms of the ratio of the drop diameter to the microscale feature center-to-center distance (d_{drop}/P), (c) Percentage of drops with diameters below or above the $d_{drop}/P = 2$ threshold which have departed the surface, and (d) Size distribution of drops with diameters above 30 μm for P-0, P-120, P-64, P-40, and P-30 surfaces. An individual point refers to the percentage of total drops on the surface that have diameters within 30 μm interval starting at the value of the point.

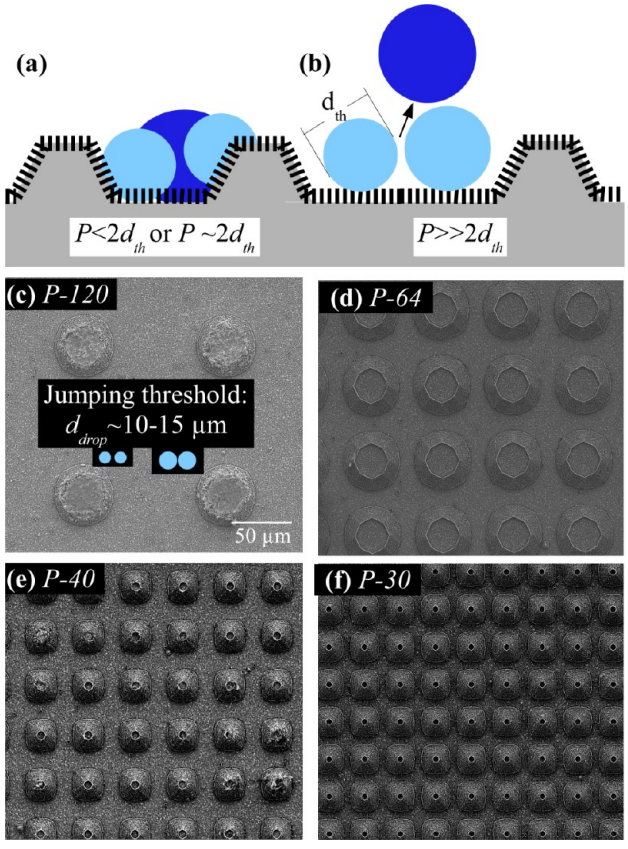

Figure 9. Schematic showing the relation between postcoalescence mobility of droplets with $d_{drop}/P = 2$ on hierarchical SHS with the center-to-center distance of the microscale topological features (P) (a) equal to or smaller and (b) greater than two times the mobile coalescence threshold diameter (d_{th}); (c–f) top-down SEM images of P-120, P-64, P-40, and P-30 surfaces and schematic showing two pairs of drops with diameters of 10 and 15 μm.

the area is occupied by large droplets in immobile micro-Wenzel state.

CONCLUSIONS

In this work we explored the relation between droplet coalescence dynamics, droplet wetting states, and the microscale topography of the underlying hierarchical SHS. We showed that for mobile coalescence to occur between two droplets on any of the SHS, the drops need to have diameters of at least 10 to 20 μm. However, we also showed that coalescence of two drops producing a drop with diameter above 30 μm is infrequent as compared to serial coalescence events involving three or more drops. The multidrop merging events occurred when neighboring droplets combined or when drops were sequentially swept up in a domino-like process. These novel droplet shedding modes were triggered by mobile coalescence resulting in a tangentially departing droplet that subsequently collided with another neighboring or distant drop. Irrelevant of the mode, the serial coalescence events culminated in formation of a drop that either departed or remained anchored to the surface. Analysis of postmerging adhesion of drops with diameters in the 30–100, 100–200, and above 200 μm ranges demonstrated strong influence of the microscale feature geometry; however no clear trend was evident from the data presented in these absolute terms. To gain an insight into the postmerging adhesion data, we studied the effect of the microscale topology on the wetting states of the condensed droplets. We confirmed that microdroplets can be in nano-Wenzel and nano-Cassie states, dependent on the location of nanodroplet nucleation on the nanostructure. The capillary bridges connecting droplets in the nano-Wenzel state to the substrate were likely responsible for occurrence of immobile coalescences between two small microdrops. Next, we found that drops condensed on hierarchical SHS with microscale feature center-to-center distance equal or less than 64 μm did transition into the micro-Cassie state. In order to transition into this microscale nonwetting state the drops had to have

dx.doi.org/10.1021/la304264g | Langmuir 2013, 29, 881–891

diameters two to three times greater than the center-to-center distance between the microscale topological features. Rescaling of the postmerging drop adhesion data in terms of merged diameter to microscale feature center-to-center distance ratio revealed clear trends. Specifically, if a hierarchical SHS architecture did not promote formation of drops in the micro-Cassie state, the postmerging drop adhesion was dramatically increased as compared to solely nanostructured surface. In turn, on micro-Cassie state enabling architectures about 20−25% of droplets with $d_{drop}/P > 2$ departed after merging with other drops. The formation of drops in a micro-Cassie state also correlated to a decrease in the maximum observed diameter from ∼1000 μm to ∼500 μm (P-0 and P-120 vs P-64, P-40, and P-30 SHS). For droplets with $d_{drop}/P < 2$, about 25−35% of drops formed in a drop merging event departed the P-0, P-120, P-40, and P-30 SHS, while 60% departed the P-64 SHS. The architecture of the P-64 surface is optimal for shedding microdroplets because it enables higher mobility of droplets with $d_{drop}/P > 2$ through formation of Cassie state while at the same time provides sufficient spacing in-between the microscale features for mobile coalescence of two droplets with diameters above d_{th}.

■ ASSOCIATED CONTENT

Supporting Information

Movies of all condensation experiments performed in the paper, definitions of wetting parameters, and analysis of mobile and immobile coalescence on all of the SHS and postmerging drop adhesion data in terms of d_{drop}/P ratio. This material is available free of charge via the Internet at http://pubs.acs.org.

■ AUTHOR INFORMATION

Corresponding Author

*E-mail: konradr@mit.edu; varanasi@mit.edu.

Notes

The authors declare no competing financial interest.

■ ACKNOWLEDGMENTS

K.K.V. gratefully acknowledges the NSF Career Award (0952564) and the Dupont-MIT Alliance for funding this work. Z.W. gratefully acknowledges financial support from the City University of Hong Kong under Strategic Research Grants 7008090 and 7002705. Part of this work was performed using facilities at National Institute of Standards and Technology in Gaithersburg, MD.

■ REFERENCES

(1) Beer, J. M. High Efficiency electric power generation: The Environmental Role. *Prog. Energy Combust. Sci.* **2007**, *33*, 107−134.

(2) Dietz, C.; Rykaczewski, K.; Fedorov, A. G.; Joshi, Y. Visualization of droplet departure on a superhydrophobic surface and implications to heat transfer enhancement during dropwise condensation. *Appl. Phys. Lett.* **2010**, *97*, 033104.

(3) Varanasi, K. K.; Hsu, M.; Bhate, N.; Yang, W.; Deng, T. Spatial control in the heterogeneous nucleation of water. *Appl. Phys. Lett.* **2009**, *95*, 094101.

(4) Kim, M. H.; Bullard, C. W. Air-side Performace of Brazed Aluminium Het Exchangers under Dehumidifying Conditions. *Int. J. Refrigeration* **2002**, *25*, 924−934.

(5) Khawaji, A. D.; Kutubkhanah, I. K.; Wie, J. M. Advances in Seawater Desalination Technologies. *Desalination* **2008**, *221*, 47−69.

(6) Humplik, T.; Lee, J.; O'Hern, S. C.; Fellman, B. A.; Baig, M. A.; Hassan, S. F.; Atieh, M. A.; Rahman, F.; Laoui, T.; Karnik, R.; Wang, E. N. Nanostructured materials for water desalination. *Nanotechnology* **2011**, *22*, 292001−292020.

(7) Nikolayev, V. S.; Beysens, D.; Gioda, A.; Milimouka, I.; Katiushin, E.; Morel, J. P. Water recovery from dew. *J. Hydrol.* **1996**, *182*, 19−35.

(8) Beysens, D. Dew nucleation and growth. *Comp. Rend. Phys.* **2006**, *7*, 1082−1100.

(9) Beysens, D. The formation of dew. *Atmos. Res.* **1995**, *39*, 215−237.

(10) Yu, T. S.; Park, J.; Lim, H.; Breuer, K. S. Fog Deposition and Accumulation on Smooth and Textured Hydrophobic Surfaces. *Langmuir* **2012**, *28*, 12771−12778.

(11) Lee, A.; Moon, M.-W.; Lim, H.; Kim, W.-D.; Kim, H.-Y. Water harvest via dewing. *Langmuir* **2012**, *28*, 10183−10191.

(12) Andrews, H. G.; Eccles, E. A.; Schofield, W. C. E.; Badyal, J. P. S. Three-Dimensional Hierarchical Structures for Fog Harvesting. *Langmuir* **2011**, *27*, 3798−3802.

(13) Rose, J. W. On mechanism of dropwise condensation. *Int. J. Heat Mass Transf.* **1967**, *10*, 755−765.

(14) Lefevre, E. J.; Rose, J. W. A theory of heat transfer by dropwise condensation. *In Proc. 3rd Int. Heat Transfer Conf.*, Chicago, 1966; 362-375.

(15) Schmidt, E.; Schurig, W.; Sellschopp, W. Versuche über die Kondensation von Wasserdampf in Film- und Tropfenform. *Forschung Ingenieurwesen* **1930**, *1*, 53−63.

(16) Rose, J. W. Dropwise condensation theory and experiment: a review. *Proc. Inst. Mech. Eng. A* **2002**, *216*, 115−128.

(17) McCormick, J. L.; Westwater, J. W. Drop dynamics and heat transfer during dropwise condensation of water vapor. *Chem. Eng. Prog. Symp. Ser.* **1966**, *62*, 120−134.

(18) Umur, A.; Griffith, P. Mechanism of dropwise condensation. *J. Heat Transfer* **1965**, *87*, 275−282.

(19) Glicksman, L. R.; Hunt, A. W. Numerical Simulation of Dropwise Condensation. *Int. J. Heat Mass Transf.* **1972**, *15*, 2251−2269.

(20) Chen, C. H.; Cai, Q. J.; Tsai, C. L.; Chen, C. L.; Xiong, G. Y.; Yu, Y.; Ren, Z. F. Dropwise condensation on superhydrophobic surfaces with two-tier roughness. *Appl. Phys. Lett.* **2007**, *90*, 173108.

(21) Dorrer, C.; Ruhe, J. Wetting of silicon nanograss: From superhydrophilic to superhydrophobic surfaces. *Adv. Mater.* **2008**, *20*, 159−163.

(22) Rykaczewski, K.; Chinn, J.; Walker, L. A.; Scott, J. H. J.; Chinn, A. M.; Jones, W.; Hao, C.; Yao, S.; Wang, Z. How nanorough is rough enough to make a surface superhydrophobic during condensation? *Soft Matter* **2012**, *8*, 8786−8794.

(23) Boreyko, J. B.; Chen, C. H. Self-Propelled Dropwise Condensate on Superhydrophobic Surfaces. *Phys. Rev. Lett.* **2009**, *103*, 184501.

(24) Wang, F.-C.; Yang, F.; Zhao, Y.-P. Size effect on the coalescence-induced self-propelled droplet. *Appl. Phys. Lett.* **2011**, *98*, 053112.

(25) Rykaczewski, K.; Scott, J. H. J.; Rajauria, S.; Chinn, J.; Chinn, A. M.; Jones, W. Three dimensional aspects of droplet coalescence during dropwise condensation on superhydrophobic surfaces. *Soft Matter* **2011**, *7*, 8749−8752.

(26) Rykaczewski, K.; Chinn, J.; Walker, M. L.; Scott, J. H. J.; Chinn, A.; Jones, W. Dynamics of Nanoparticle Self Assembly into Superhydrophobic Liquid Marbles during Water Condensation. *ACS Nano* **2011**, *5*, 9746−9754.

(27) Chen, X.; Wu, J.; Ma, R.; Hua, M.; Koratkar, N.; Yao, S.; Wang, Z. Nanograssed Micropyramidal Architectures for Continuous Dropwise Condensation. *Adv. Funct. Mater.* **2011**, *21*, 4617−4623.

(28) He, M.; Zhou, X.; Zeng, X.; Cui, D.; Zhang, Q.; Chen, J.; Li, H.; Wang, J.; Cao, Z.; Song, Y.; Jiang, L. Hierarchically structured porous aluminum surfaces for high-efficient removal of condensed water. *Soft Matter* **2012**, *8*, 2680−2683.

(29) Feng, J.; Qin, Z.; Yao, S. Factors Affecting the Spontaneous Motion of Condensate Drops on Superhydrophobic Copper Surfaces. *Langmuir* **2012**, *28*, 6067−6075.

(30) Boreyko, J. B.; Zhao, Y.; Chen, C.-H. Planar jumping-drop thermal diodes. *Appl. Phys. Lett.* **2011**, *99*, 234105.
(31) Tanasawa, I. Critical size of departing drops. *Proc. 5th Inter. Heat Transfer Conf.* **1974**, 188.
(32) Rose, J. W. Some aspects of condensation heat transfer theory. *Int. Comm. Heat Mass Trans.* **1988**, *15*, 449−473.
(33) Miljkovic, N.; Enright, R.; Wang, E. Effect of Droplet Morphology on Growth Dynamics and Heat Transfer during Condensation on Superhydrophobic Nanostructured Surfaces. *ACS Nano* **2012**, *6*, 1776−1785.
(34) Enright, R.; Miljkovic, N.; Al-Obeidi, A.; Thompson, C. V.; Wang, E. N. Condensation on superhydrophobic surfaces: The role of local energy barriers and structure length-scale. *Langmuir* **2012**, *28*, 14424−14432.
(35) Rykaczewski, K. Microdroplet Growth Mechanism during Water Condensation on Superhydrophobic Surfaces. *Langmuir* **2012**, *28*, 7720−7729.
(36) Liu, T.; Sun, W.; Sun, X.; Ai, H. Thermodynamic Analysis of the Effect of the Hierarchical Architecture of a Superhydrophobic Surface on a Condensed Drop State. *Langmuir* **2010**, *26*, 14835−14841.
(37) Wenzel, R. N. Resistance of Solids Surfaces to Wetting by Water. *Ind. Eng. Chem.* **1936**, *28*, 988−994.
(38) Cassie, A. B. D.; Baxter, S. Wettability of porous surfaces. *Trans. Faraday Soc.* **1944**, *40*, 546−551.
(39) Liu, T. Q.; Sun, W.; Sun, X. Y.; Ai, H. R. Mechanism Study of Condensed Drops Jumping on Super-Hydrophobic Surfaces. *Colloids Surf., A* **2012**, *414*, 366−374.
(40) Quéré, D. Non-sticking drops. *Rep. Prog. Phys.* **2005**, *68*, 2495−2532.
(41) Quéré, D. Wetting and Roughness. *Ann. Rev. Mater. Res.* **2008**, *38*, 71−99.
(42) Nosonovsky, M.; Bhushan, B. Patterned Nonadhesive Surfaces: Superhydrophobicity and Wetting Regime Transitions. *Langmuir* **2007**, *24*, 1525−1533.
(43) Nosonovsky, M.; Bhushan, B. Biomimetic Superhydrophobic Surfaces:a Multiscale Approach. *Nano Lett.* **2007**, *7*, 2633−2637.
(44) Koch, K.; Bohn, H. F.; Barthlott, W. Hierarchically Sculptured Plant Surfaces and Superhydrophobicity. *Langmuir* **2009**, *25*, 14116−14120.
(45) Su, Y.; Ji, B.; Huang, Y.; Hwang, K.-c. Nature's Design of Hierarchical Superhydrophobic Surfaces of a Water Strider for Low Adhesion and Low-Energy Dissipation. *Langmuir* **2010**, *26*, 18926−18937.
(46) Kwon, H.-M.; Paxson, A. T.; Varanasi, K. K.; Patankar, N. A. Rapid Deceleration-Driven Wetting Transition during Pendant Drop Deposition on Superhydrophobic Surfaces. *Phys. Rev. Lett.* **2011**, *106*, 036102.
(47) Patankar, N. A. Mimicking the Lotus Effect: Influence of Double Roughness Structures and Slender Pillars. *Langmuir* **2004**, *20*, 8209−8213.
(48) Li, W.; Amirfazli, A. Hierarchical structures for natural superhydrophobic surfaces. *Soft Matter* **2008**, *4*, 462−466.
(49) Su, Y.; Ji, B.; Zhang, K.; Gao, H.; Huang, Y.; Hwang, K. Nano to Micro Structural Hierarchy Is Crucial for Stable Superhydrophobic and Water-Repellent Surfaces. *Langmuir* **2010**, *26*, 4984−4989.
(50) Sajadinia, S. H.; Sharif, F. Thermodynamic analysis of the wetting behavior of dual scale patterned hydrophobic surfaces. *J. Colloid Interface Sci.* **2010**, *344*, 575−583.
(51) Liu, H. H.; Zhang, H. Y.; Li, W. Thermodynamic Analysis on Wetting Behavior of Hierarchical Structured Superhydrophobic Surfaces. *Langmuir* **2011**, *27*, 6260−6267.
(52) Extrand, C. W. Repellency of the Lotus Leaf: Resistance to Water Intrusion under Hydrostatic Pressure. *Langmuir* **2011**, *27*, 6920−6925.
(53) Yu, Y.; Zhao, Z.-H.; Zheng, Q.-S. Mechanical and Superhydrophobic Stabilities of Two-Scale Surfacial Structure of Lotus Leaves. *Langmuir* **2007**, *23*, 8212−8216.
(54) Lee, C.; Kim, C.-J. C. Maximizing the Giant Liquid Slip on Superhydrophobic Microstructures by Nanostructuring Their Sidewalls. *Langmuir* **2009**, *25*, 12812−12818.
(55) Bittoun, E.; Marmur, A. The Role of Multi-Scale Roughness in the Lotus Effect: Is it essential for Super-Hydrophobicity? *Langmuir* **2012**, submitted.
(56) Cui, Y.; Paxson, A. T.; Smyth, K. M.; Varanasi, K. K. Hierarchical Polymeric Textures via Solvent-Induced Phase Transformation: A Single-Step Production of Large-Area Superhydrophobic Surfaces. *Colloids Surf., A* **2012**, *394*, 8−13.
(57) McCarthy, M.; Gerasopoulos, K.; Enright, R.; Culver, J. N.; Ghodssi, R.; Wang, E. N. Biotemplated hierarchical surfaces and the role of dual length scales on the repellency of impacting droplets. *Appl. Phys. Lett.* **2012**, *100*, 263701−5.
(58) Verho, T.; Bower, C.; Andrew, P.; Franssila, S.; Ikkala, O.; Ras, R. H. A. Mechanically Durable Superhydrophobic Surfaces. *Adv. Mater.* **2010**, *23*, 673−678.
(59) Verho, T.; Korhonen, J. T.; Sainiemi, L.; Jokinen, V.; Bower, C.; Franze, K.; Franssila, S.; Andrew, P.; Ikkala, O.; Ras, R. H. A. Reversible switching between superhydrophobic states on a hierarchically structured surface. *Proc. Natl. Acad. Sci. U.S.A.* **2012**, DOI: 10.1073/pnas.1204328109.
(60) Narhe, R. D.; Beysens, D. A. Nucleation and Growth on a Superhydrophobic Grooved Surface. *Phys. Rev. Lett.* **2004**, *93*, 076103.
(61) Narhe, R. D.; Beysens, D. A. Water condensation on a superhydrophobic spike surface. *Europhys. Lett.* **2006**, *75*, 98−104.
(62) Narhe, R. D.; Beysens, D. A. Growth dynamics of water drops on a square-pattern rough hydrophobic surface. *Langmuir* **2007**, *23*, 6486−6489.
(63) Narhe, R. D.; González-Viñas, W.; Beysens, D. A. Water condensation on zinc surfaces treated by chemical bath deposition. *Appl. Surf. Sci.* **2011**, *256*, 4930−4933.
(64) Wier, K. A.; McCarthy, T. J. Condensation on Ultrahydrophobic Surfaces and Its Effect on Droplet Mobility: Ultrahydrophobic Surfaces Are Not Always Water Repellant. *Langmuir* **2006**, *22*, 2433−2436.
(65) Dorrer, C.; Ruhe, J. Contact Line Shape on Ultrahydrophobic Post Surfaces. *Langmuir* **2007**, *23*, 3179−3183.
(66) Dorrer, C.; Ruhe, J. Condensation and Wetting Transitions on Microstructured Ultrahydrophobic Surfaces. *Langmuir* **2007**, *23*, 3820−3824.
(67) Cheng, Y.-T.; Rodak, D. E. Is the lotus leaf superhydrophobic? *Appl. Phys. Lett.* **2005**, *86*, 144101.
(68) Jung, Y. C.; Bhushan, B. Wetting behaviour during evaporation and condensation of water microdroplets on superhydrophobic patterned surfaces. *J. Microsc.-Oxf.* **2008**, *229*, 127−140.
(69) Choi, C.-H.; Kim, C.-J. Fabrication of a dense array of tall nanostructures over a large sample area with sidewall profile and tip sharpness control. *Nanotechnology* **2006**, *17*, 5326.
(70) Rykaczewski, K.; Scott, J. H. J.; Fedorov, A. G. Electron beam heating effects during environmental scanning electron microscopy imaging of water condensation on superhydrophobic surfaces. *Appl. Phys. Lett.* **2011**, *98*, 093106.
(71) Rykaczewski, K.; Scott, J. H. J. Methodology for imaging nano-to-microscale water condensation dynamics on complex nanostructures. *ACS Nano* **2011**, *5*, 5926−5968.
(72) Anand, S.; Son, S. Y. Sub-Micrometer Dropwise Condensation under Superheated and Rarefied Vapor Condition. *Langmuir* **2010**, *26*, 17100−17110.
(73) Rasband, W. S. ImageJ. http://rsb.info.nih.gov/ij/.
(74) Beysens, D.; Knobler, C. M. Growth of Breath Figures. *Phys. Rev. Lett.* **1986**, *57*, 1433−1436.
(75) Rykaczewski, K.; Landin, T.; Walker, L. A.; Scott, J. H. J.; Varanasi, K. K. Direct Nano-to-Microscale Imaging of Complex Interfaces Involving Solid, Liquid, and Gas Phases. *ACS Nano* **2012**, *6*, 9326−9334.
(76) Ma, X.; Wang, S.; Lan, Z.; Peng, B.; Ma, H. B.; Cheng, P. Wetting Mode Evolution of Steam Dropwise Condensation on

Superhydrophobic Surface in the Presence of Noncondensable Gas. *J. Heat Transfer* **2012**, *134*, 021501−021509.